Reproducible gray-box neural network for predicting the fragility index and the temperature-dependency of viscosity

Daniel R. Cassar

Department of Materials Engineering, Federal University of São Carlos, São Carlos, Brazil

Abstract

The temperature-dependence of the viscosity of a liquid is relevant in many scientific and technological fields, for example, it is critical to adjust process variables for glass making. The current trend in glass science is building reliable models for property prediction to accelerate glass development. Recently, Tandia and co-authors developed a gray-box neural network model with high performance; they connected the pattern recognition of neural networks with a physical model, the MYEGA equation. Similarly, the aim of this work was to use the SciGlass database to build an open-source gray-box model to predict viscosity. The viscosity dataset used had about 130 000 examples with 28 different chemical elements. This new gray-box model included a pre-processing unit that extracts and scales chemical features before feeding them to the neural network. The best model (after hyperparameter tuning) had a coefficient of determination (R^2) of 0.987 and root mean squared error (RMSE) of 0.59, both computed for the holdout dataset, which was not used for training. In addition to the temperature-dependence of viscosity, the fragility index of the liquid can also be computed by the gray-box model. The hope is that this free and open framework for property prediction can be used and improved by the community to accelerate the development of new materials.

Keywords: viscosity, neural network, machine learning, property prediction, feature extraction

1. Introduction

Viscosity is one of the most important properties of disordered matter. In the context of oxide glass-forming liquids, the temperature-dependence of viscosity is used to adjust process variables for glass making, including conformation and annealing [1]; it can also be used as a proxy for the diffusion coefficient for kinetic processes such as crystal nucleation and crystal growth [2–5]. Recently, a new parameter of glass-forming ability was proposed based on the viscosity at the liquidus temperature [6].

Reliable predictive models are desired in practically all fields of materials science and engineering [7], including glass science and technology [8]. These predictive models are expected to increase the speed and reduce the cost for developing new materials. This desire has increased the interest in the interface between machine learning and oxide glass science, as seen in a recent surge of publications in this topic [9–12]. In this context, the most used machine learning technique by far is neural networks (NN) [9, 12–26], which are particularly good at finding patterns and modeling non-linear dependencies between a set of features (input) and targets (output). The usual approach found in the literature is to use a feedforward NN as a "universal regressor" model to predict glass properties, and is often referred to as a "black-box", given the difficulty of interpreting the internal rules of the model. Fig 1 shows a flowchart of this black-box approach for predicting viscosity.

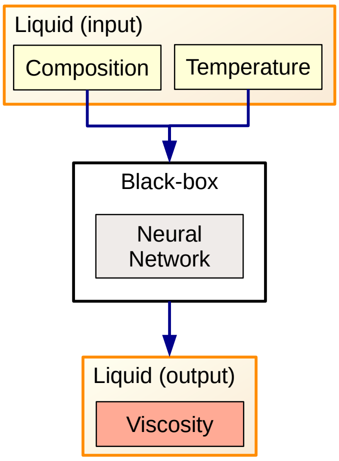

Figure 1: Flowchart of the use of a neural network as a black-box predictor of viscosity.

Recently, Tandia et al. [12] developed a gray-box approach to predict viscosity: they embedded a physical model in the machine learning pipeline, which also contains a neural network. Compared with the black-box approach, this strategy changes the purpose of the NN from

*Corresponding author
Email address: contact@danielcassar.com.br (Daniel R. Cassar)

a predictor of viscosity to a predictor of the *parameters* of a viscosity model, which in this case was the MYEGA equation [27] (shown in Eq. (1), where η is the viscosity, T the absolute temperature, and A, C, and K are adjustable parameters). The gray-box approach improved the prediction of viscosity when compared with the black-box approach [12].

$$\eta\left(T\right) = A \exp\left(\frac{C}{T} \exp\left(\frac{K}{T}\right)\right) \quad (1)$$

The aim of this work was to build and test a reproducible gray-box NN to predict the temperature-dependence of viscosity. This work includes (a) a pre-processing operation with a chemical feature extractor and a normalization unit, (b) an extended chemical domain of 28 chemical compounds, and (c) a permissive license that allows the community to use and improve both data and code (see Section (3.4)).

2. Materials and methods

2.1. Data collection and preparation

Data used in this work come from the SciGlass database, which is publicly available under the Open Database License (https://github.com/epam/SciGlass). This database collects viscosity data following two different strategies:

- the first is by reporting the temperature where the viscosity is equal to a particular value. The temperature T_{12}, for example, is where viscosity is equal to 10^{12} Pa s;
- the second is by reporting the viscosity measured at a particular temperature. The viscosity η_{873}, for example, was obtained at 873 K.

The dataset containing all SciGlass viscosity data has more than 170 000 entries, each one with the chemical composition, temperature, and the respective viscosity at that temperature. Data collected following the aforementioned two strategies have many duplicated entries, with the same composition measured at the same temperature. Thus, to avoid data leakage [28] during the training of the model, a deduplication routine was applied to the dataset by following three steps:

1. rounding the chemical composition (in mole fraction) to the 3rd decimal place, and the temperature (in Kelvin) to the closest integer;
2. grouping the examples with the same chemical composition and temperature;
3. taking the median value of the base-10 logarithm of viscosity for each group, thus creating a new dataset with only one example per group.

The deduplicated dataset was further filtered to contain only those liquids made with one or more of the following 28 oxide components (those in bold were also considered in by Tandia et al. [12]): $\mathbf{Al_2O_3}$, As_2O_3, $\mathbf{B_2O_3}$, **BaO**, Bi_2O_3, **CaO**, CdO, Cr_2O_3, Fe_2O_3, FeO, GeO_2, $\mathbf{K_2O}$, La_2O_3, Li_2O, **MgO**, MnO, $\mathbf{Na_2O}$, P_2O_5, PbO, SO_3, Sb_2O_3, SiO_2, $\mathbf{SnO_2}$, **SrO**, TiO_2, Y_2O_3, ZnO, and ZrO_2. These particular compounds are the oxides with the largest number of examples, and they all contain chemical elements with the necessary data available for feature extraction (see Section 2.2.2).

After filtering, all examples with a viscosity above 10^{12} Pa s were removed, because these data points are more likely to not having been measured in equilibrium conditions.

The final dataset containing 134 638 examples was then divided into the *training set* (80 % of the data) and the *holdout set* (20 % of the data). The holdout set was used to access the uncertainty of prediction of the trained model, and thus it was *not* used for the routine of hyperparameter tuning (see Section 2.2.3). However, the final model was trained with all the data (training *and* holdout sets), as this is the standard procedure for building the final predictive model. All calculations were performed in the base-10 logarithmic scale of viscosity due to the immense difference between the lowest and highest value of viscosity in this dataset (13 orders of magnitude).

2.2. Machine learning pipeline

2.2.1. Overview

"Neural network" is a general term for a group of machine learning algorithms used for pattern recognition, which is performed by an assortment of interconnected computational units called neurons. In materials science, NNs can be applied in many types of problems and are often used for their "universal regressor" capabilities. This work focuses on feedforward multilayer perceptron NNs, one of the most simple architectures of NNs. For more information about the mathematical and statistical basis of this topic, see [29].

This work was based on the gray-box NN approach recently published by Tandia et al. [12]. A new item proposed and tested here is an additional step in the pipeline: a pre-processing step that includes a feature extractor and a scaler. The feature extractor will be described in Section 2.2.2; the scaler is a unit that computes the z-score of the features supplied to the NN to reduce the bias of those features with a higher magnitude (see the Appendix for more information on the z-score).

Figure 2 shows a flowchart of the gray-box pipeline used here. The arrows indicate the flow of information that starts from the composition and the temperature of the liquid (input) and ends with the prediction of its viscosity (output). The parameters A, C, and K of the MYEGA equation are temperature-independent in the original publication [27]; however, Tandia et al. [12] tested training a NN that receives both the composition and the temperature as features, effectively making A, C, and K temperature-dependent. Here, both approaches were tested. When the MYEGA parameters are temperature-independent, the dashed arrow in Fig. 2 is not allowed to pass information, and the pipeline is called “Gray-box 1”. When the MYEGA parameters are temperature-dependent, the dashed arrow in Fig. 2 is allowed to pass information, and the pipeline is called “Gray-box 2”.

Finally, the gray-box approach allows us to have access to the viscosity function $\eta(T)$ of a particular liquid. With this function, we can compute the liquid fragility index m (as defined by Angell [30]) and its T_{12}, the latter being a temperature reasonably close to the laboratory glass transition temperature. The mathematical definitions of these properties are:

$$m \equiv \left.\frac{\partial \eta(T)}{\partial (T_{12}/T)}\right|_{T=T_{12}}, \tag{2}$$

and

$$\eta(T_{12}) \equiv 10^{12}\,\text{Pa.s.} \tag{3}$$

2.2.2. Feature extraction

Neural networks that use only the chemical composition domain for the features may have poor performance for predictions reasonably outside of the training domain. A strategy that may overcome this limitation is changing the feature domain. In this work, this was performed by leveraging the knowledge of the chemical properties of the elements.

In the *chemical composition* domain, the features of a liquid are represented by a vector with the atomic mole fraction of its constituents. To convert these features to the *chemical property* domain, one must choose a chemical property and an aggregator function. An example is to choose the atomic weight as property and compute the “mean atomic weight”, which is a feature of the liquid. By choosing different chemical properties and aggregator functions, one can “extract” new features from the liquid in the chemical property domain. This procedure is called feature extraction or feature engineering.

The mathematical procedure for this process starts by creating the vector $\boldsymbol{C} = [x_1, x_2, \ldots, x_n]$ of the atomic mole fractions of the chemical elements e_1, e_2, …, e_n that make a certain liquid. Let $\boldsymbol{S} = [s_1, s_2, \ldots, s_n]$ be the vector of a certain chemical property s_i of the chemical element e_i (the atomic weight, for example). We compute the property vectors $\boldsymbol{W}$ (weighted) and $\boldsymbol{A}$ (absolute) as

$$\boldsymbol{W} = \boldsymbol{C}\boldsymbol{S}^T, \tag{4}$$

and

$$\boldsymbol{A} = \lceil \boldsymbol{C} \rceil \boldsymbol{S}^T. \tag{5}$$

Please note that the ceil function is applied element-wise in vector $\boldsymbol{C}$ in Eq. (5).

Finally, by applying an aggregator function to the items of the vectors $\boldsymbol{W}$ or $\boldsymbol{A}$, we obtain a particular chemical feature of the liquid. The aggregator functions used in this work are summation (sum), mean, standard deviation (std), minimum (min), and maximum (max).

Many features can be extracted following this procedure. In this work, the chemical features considered were atomic number, weight, and volume; atomic radius reported by Slater and Rahm [31–33]; boiling and melting points; C_6 coefficient reported by Gould and Bučko [34]; single- and double-bond covalent radius reported by Pyykko [35, 36]; density; dipole polarizability; number of electrons, neutrons, and protons; electronegativity in the Gosh and Pauling scales [37, 38]; Glawe’s, Mendeleev’s, and Pettifor’s numbers [39, 40]; heat of formation; lattice constant; mass number of the most abundant isotope; and Van der Walls radius reported by Haynes, Alvarez, Batsanov, and from the MM3 and Universal force fields [38, 41–44]. All these chemical properties are available in the Python module `mendeleev` [45].

A benefit of using chemical properties instead of chemical composition is that the model can predict the viscosity of liquids composed of chemical elements not present in the training dataset, the only requirement being that the chemical properties of said elements are available. With the strategy used here, 62 elements can be considered for viscosity prediction (those in bold were present in the training dataset): Ag, **Al**, **As**, Au, **B**, **Ba**, Be, **Bi**, Br, C, **Ca**, **Cd**, Cl, Co, **Cr**, Cs, Cu, **Fe**, Ga, **Ge**, Hf, Hg, I, In, Ir, **K**, **La**, **Li**, **Mg**, **Mn**, Mo, N, **Na**, Nb, Ni, **O**, Os, **P**, **Pb**, Pd, Pt, Rb, Re, Rh, Ru, **S**, **Sb**, Sc, Se, **Si**, **Sn**, **Sr**, Ta, Tc, Te, **Ti**, Tl, V, W, **Y**, **Zn**, and **Zr**.

Only chemical features were extracted in this work. However, in the framework proposed by Adam and Gibbs [46] (which is the basis for the MYEGA equation), they argue that viscosity depends on the size of the cooperative rearranging regions in the liquid, which are related to the atomic structure of the liquid. Therefore, a predictor of viscosity that uses only chemical features is unlikely to generalize *all* the intricacies of viscous flow. Structural features, however, are outside of the scope of this work.

2.2.3. Hyperparameters

The prediction power and generalization of a neural network are highly dependent on its hyperparameters (HP), such as the number of neurons, number of layers, activation function, and others. It is not trivial to determine a good set of HP for a new problem. Because of this, before settling for the final network architecture, it is vital to test some sets of HP , a process called *hyperparameter tuning*.

HP tuning was performed using the `hyperopt` Python module [47] guided by suggestions made by a Tree-structured Parzen Estimator (TPE) algorithm [48]. The training set (see the last paragraph of Section 2.1) was divided into five folds. Four of these folds were used for training the NN (10 % of which were selected for validation). The remaining fold was used for testing. The score that guided the TPE algorithm was the mean squared error (MSE) loss of the testing set.

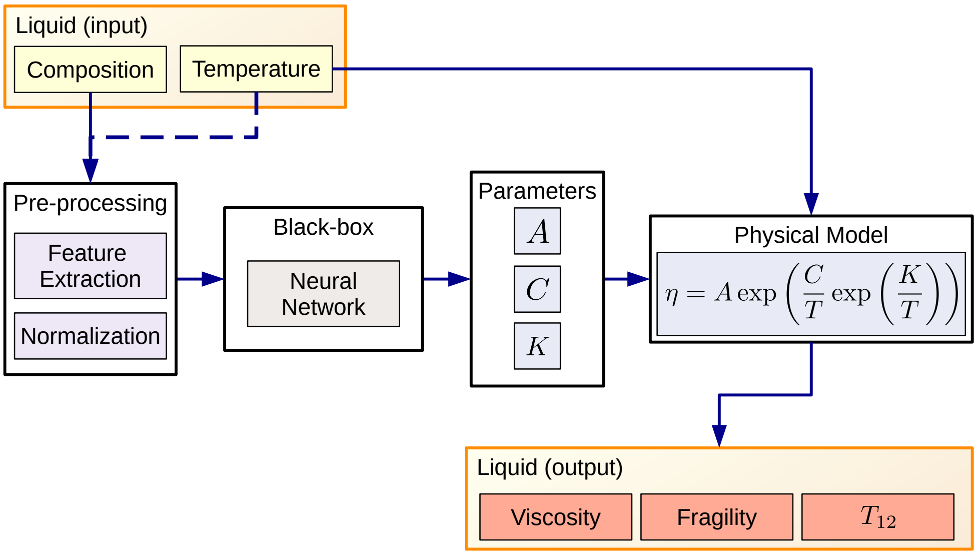

Figure 2: Flowchart of the machine learning pipeline used in this work.

Table 1: Hyperparameters search spaces. The functions Tanh and ReLU are the hyperbolic tangent and the rectifier linear unit. Learning rate and momentum are parameters of the stochastic gradient descent (SGD) optimization algorithm used for backpropagation [49, 50]. More information on the early stopping routine can be found in the Appendix.

Hyperparameter	Search space
Number of hidden layers (fixed)	1
Maximum number of neurons per layer	128
Minimum number of neurons per layer	1
Hidden layers activation function	Tanh or ReLU
Training batch size	16, 32, 64, 128, or 256
Patience of early stopping routine (integer)	[0, 15]
Number of chemical features (integer)	[4, 99]
SGD learning rate	$[10^{-6}, 10^{-2}]$
SGD momentum	[0, 1]

Table 1 shows the search space that was considered in the HP tuning routine, for which a total of 200 different sets of HP were sampled and tested. The choice to use one hidden layer is based on the architecture reported by Tandia et al.. [12]. Prior tests with more hidden layers (not shown) also supported the choice of one hidden layer.

The 20 HP sets with the lowest MSE loss were selected from the 200 HP sets sampled. For the selected sets, 5-fold cross-validation was performed, and the average value of the five losses was computed. The HP set with the lowest average MSE loss in this analysis was selected as the final architecture for the neural network.

One of the hyperparameters considered in this tuning process was the number of chemical features that will be supplied to the NN. A total of 290 different chemical features per liquid were extracted following the procedure discussed in Section 2.2.2. Adding more features to a neural network can improve the prediction; however, it may be detrimental to the network's generalization, as it may try to find spurious patterns, which lead to overfitting. This issue is why the number of chemical features was limited and considered a hyperparameter for tuning.

Different chemical features may be more or less relevant for predicting viscosity. Before starting the HP tuning routine, the features of the problem were ranked according to their relevance in predicting viscosity, and selected by the HP "number of chemical features" according to this rank. The ranking was performed by first inducing a random forest model using the default settings of the Python module `sklearn` [51]. This model was induced using only the training dataset, and the features were ranked by their importance score in descending order. Temperature is a feature but not a *chemical* feature, hence it was always considered in the machine learning pipeline because it is necessary to compute the MYEGA equation. The chemical features used in the final NN architecture are reported in the Appendix.

2.3. Experiments

Two experiments were tested in this work, namely the Gray-box 1 and Gray-box 2, as defined in Section 2.2.1. The aim was to test if the performance of the pipeline improves by using temperature as a feature for the NN.

All experiments were coded in the Python programming language, and the NN were trained using a personal computer with an 8-core CPU and 16 GB of RAM. The neural networks were built using the `PyTorch-Lightning` module [52], a high-level interface for `PyTorch [53]`. Data management was performed with the `pandas` module [54].

The metrics used to evaluate the experiments are the coefficient of determination (R^2), the root mean squared error (RMSE), the mean absolute error (MAE), and the median absolute error (MedAE). More information on the metrics can be found in the Appendix.

Table 2: Metrics for the Gray-box 1 and Gray-box 2 experiments. The symbol ↑ indicates that the higher the metric, the better, whereas the symbol ↓ indicates the opposite.

Metric	Gray-box 1	Gray-box 2
R^2 (↑)	0.986	0.987
RMSE (↓)	0.61	0.59
MAE (↓)	0.36	0.34
MedAE (↓)	0.20	0.19

3. Results and discussion

3.1. Hyperparameters

The NN architecture with the best performance after HP tuning was the one with a single hidden layer with 128 neurons, the rectifier linear unit (ReLU) activation function, and a 3.14 % dropout probability (considered only during training). A learning rate of 1.06×10^{-5} and a momentum of 0.975 were the best parameters of the stochastic gradient descent optimization. The training batch size was 256, and the patience of the early stopping routine was set to 13. A total of 87 chemical features were considered in the pipeline.

Three noteworthy differences between the NN architecture obtained here and that reported by Tandia et al. [12] are (a) the number of neurons in the hidden layer, (b) the activation function, and (c) the use of a dropout routine. The number of neurons in the hidden layer was 128 in this work and 8 in the work of Tandia et al. [12], who mention that the architecture disclosed was not the one obtained after HP tuning; therefore, a fair comparison is not possible. Nonetheless, the the gray-box NN developed here probably has about ten times more neurons, which seems justifiable considering that it receives about ten times more features as input. The ReLU activation function was used here whereas the hyperbolic tangent activation function was used by Tandia et al. [12]; here both functions were considered during the HP tuning process, but ReLU yielded the best results. The dropout routine is a regularization technique that was used here to reduce overfitting; there is no mention of any regularization technique in the work of Tandia et al. [12].

3.2. Holistic performance of the models

For the Gray-box 1 and Gray-box 2 experiments, Table 2 shows the metrics computed for the holdout dataset, which was not used for training the models or for the HP tuning process, as discussed in Section 2.1. These metrics give us clues on how well these models can predict data that they have never "seen": they help us access the generalization capabilities of the models.

As expected, the Gray-box 2 experiment metrics were slightly better than those of the Gray-box 1. Considering that everything else was the same between these two experiments, this result supports that the NN can generalize better when temperature is also included as a feature. In the Gray-box 2 framework, however, the parameters A, C, and K of the MYEGA equation are temperature-dependent, not in agreement with the original conditions under which the MYEGA equation was developed [27].

The performance obtained here was not as good as that reported by Tandia et al. [12], who achieved an impressive R^2 value of 0.9999 and RMSE of 0.04 for their best architecture. Possible explanations for this difference are related to (a) the quality of the data, (b) the number of chemical compounds used for training, and (c) the dataset used for computation of the metrics. Tandia et al. [12] used a proprietary dataset owned by Corning Inc. that presumably has much less variance. The number of chemical compounds used for training was 9 in the work of Tandia et al. [12] and 28 in this work; it is more difficult for a model to generalize in a diverse chemical domain. The dataset used by Tandia et al. [12] for computation of the metrics was the validation dataset, not the the holdout dataset (which they called test dataset). The validation dataset is used not to change the weights and bias of the NN but to act as a "thermometer" during training to avoid overfitting. Therefore, metrics computed for the validation dataset are usually better than those computed for the holdout dataset and are not representative of the model's generalization power to new "unseen" data. The recommended practice in the field of machine learning is to report the metrics for the holdout dataset.

Figure 3 shows a 2D histogram with the correlation between the predicted and reported values of viscosity for both experiments performed in this work. The data points are not distributed homogeneously because of the data collection strategy adopted by the SciGlass database (discussed in Section 2.1), which has a bias towards data points for which $\log_{10}(\eta)$ is an integer. The insets of the plots show a histogram of the prediction residuals, which are the difference between reported and predicted values of $\log_{10}(\eta)$.

3.3. Testing the models inside and outside the training domain

The previous section gave a holistic view of the prediction capabilities of the models. This section focuses on some liquids and liquid systems to take a closer look at the predictions.

Figure 4 shows the temperature-dependence of viscosity for a liquid with a composition of the mineral diopside ($CaO \cdot MgO \cdot 2\,SiO_2$), which is of great geological interest [55] and is also relevant for crystallization studies [5, 56, 57]. The predictions of both models (Gray-box 1 and 2) are also shown. Both models are good-but-not-great predictors for the viscosity of this particular liquid. With current technology, machine learning predictors should be used as guides for the development of new materials, not as substitutes for experimental measurements.

For more insight into the models, the interested reader can generate viscosity plots similar to Fig. 4 for other liquids by leveraging the open-source nature of this work (see

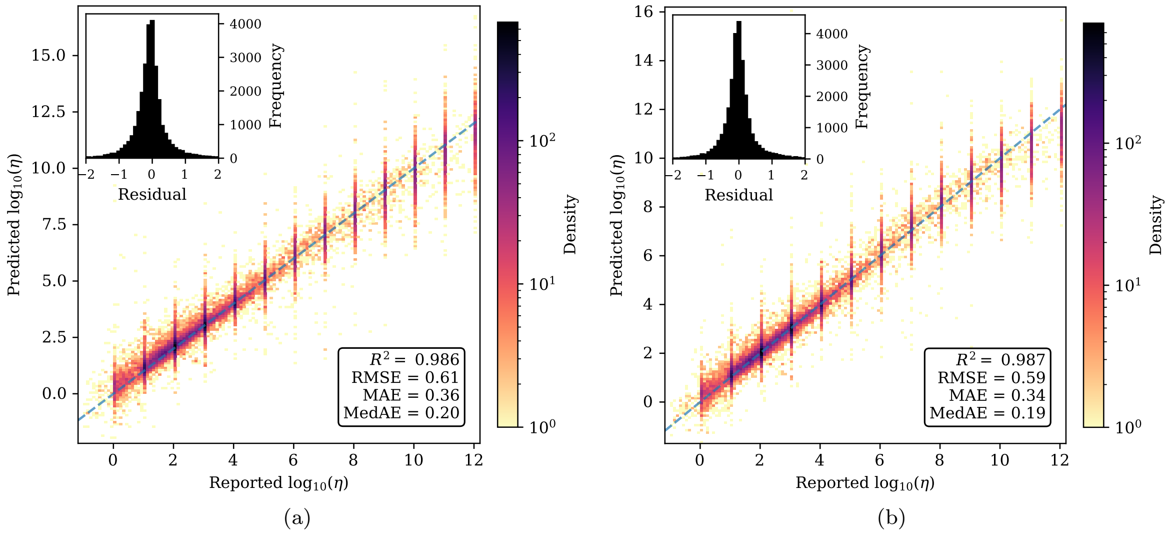

Figure 3: 2D histogram of predicted versus reported values of $\log_{10}(\eta)$ for the (**a**) Gray-box 1 experiment and the (**b**) Gray-box 2 experiment. These plots show only the holdout dataset, and each square has a corner of 0.1. The identity line is shown in dashed blue. The inset is the histogram of the residuals.

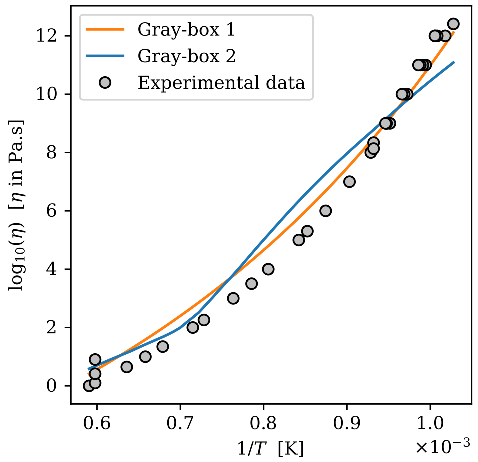

Figure 4: The logarithm of viscosity versus the inverse temperature for a liquid with a composition of diopside ($CaO \cdot MgO \cdot 2\,SiO_2$).

next section). Most liquids with composition within the training dataset showed a prediction comparable to that seen in Fig. 4. Liquids with only one component, such as silica and boron oxide, had poor prediction results, probably because structural features were not considered in the feature extraction unit. Fortunately, these single-component liquids are extensively studied and do not require a viscosity predictor.

Both models can be used to compute m and T_{12} following the definitions shown in Eqs. (2) and (3). Figure 5 shows a predicted fragility index ternary plot for the system $SiO_2{-}Na_2O{-}CaO$. As expected, the fragility has a general trend to decrease as the network becomes more connected with an increase in silica content. Interestingly, even though the fragility of liquids made with high amounts of sodium or calcium oxide is not available, the model predicts that it would be a relatively high value, close to a hundred. While the value itself is just an out-of-domain conjecture by the model, the concept of a liquid with no or small amounts of a glass-former having a high fragility index seems intuitive as only few bridging oxygen are present in the liquid.

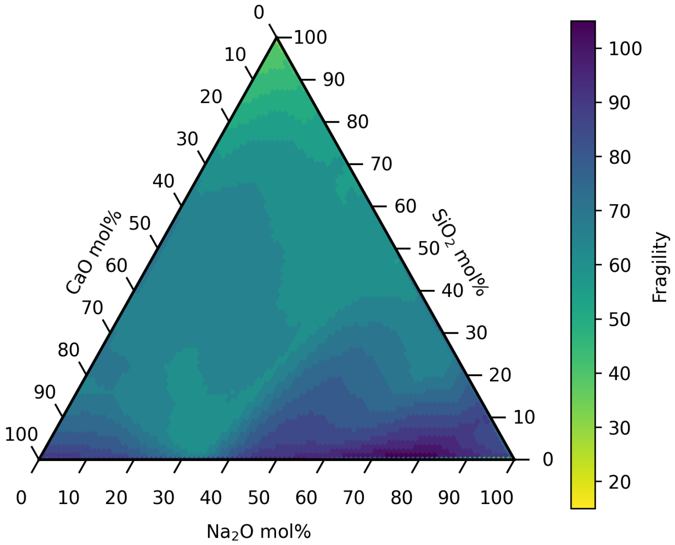

Figure 5: Fragility index ternary plot for the system $SiO_2{-}Na_2O{-}CaO$ computed using the Gray-box 1 model. Fragility values were rounded to the closest multiple of 5 for better visualization.

As already mentioned, training the NN in the chemical property domain (instead of the chemical composition domain) allows viscosity predictions of liquids having chemical elements that were not present in the training dataset. Figs. 6a and 6b show the viscosity prediction for liquids containing cobalt and rubidium, both chemical elements

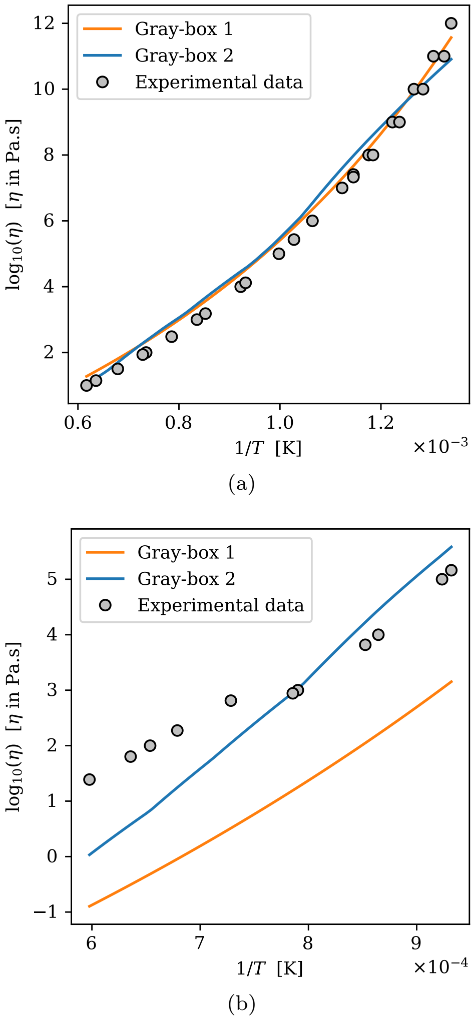

Figure 6: Prediction of the temperature-dependency of viscosity for liquids having chemical elements not included in the training dataset. (**a**) $CoO \cdot 2\,Na_2O \cdot 7\,SiO_2$. (**b**) $Rb_2O \cdot 3\,SiO_2$.

that were not part of the training composition domain. Fig. 6a shows a reasonable agreement between experimental data and prediction from both models for the liquid $CoO \cdot 2\,Na_2O \cdot 7\,SiO_2$. However, Fig. 6b shows that, for the viscosity of $Rb_2O \cdot 3\,SiO_2$, Gray-box 1 model is wrong, whereas Gray-box 2 model is reasonable in a limited temperature range. Although predictions outside the training composition domain are possible, precision may be worse when compared with compositions inside the training domain.

3.4. Reproducibility and data availability

This work was entirely performed using open-source software, as well the SciGlass database, which has a permissive license. Although the official SciGlass repository is publicly available (https://github.com/epam/SciGlass), it is not trivial to open, navigate, and extract information therein. Therefore, this work used helper functions available in the `GlassPy` Python module [58] to generate the viscosity dataset used here.

Code containing all the necessary functions to load the data and train the machine learning pipelines discussed here is available in a GitHub repository [59]. This code leverages some deterministic routines for training the NNs that are provided by the `PyTorch-Lightning` module, thus interested readers can reproduce the exact models reported here.

Due to the free and open-source nature of the code, anyone can extend the procedures presented here to better meet their needs, for example, including new features for training the models.

4. Conclusion

The aim of this work was to build a machine learning pipeline to predict the temperature-dependence of the viscosity of oxide liquids, based on a recent gray-box neural network developed by Tandia et al. [12], who embedded a physical model in the machine learning pipeline. This work introduced a pre-processing unit with a chemical feature extractor, which changes the feature domain from chemical composition to chemical properties, allowing the prediction of viscosity for liquids containing chemical elements that were not present in the training dataset.

Two experiments were proposed and tested, one considering only the chemical properties as features for the neural network, and other also considering the temperature as a feature. The first one yielded slightly worse prediction metrics, but its internal considerations are in agreement with the considerations of the physical model (the MYEGA equation). Both models can also be used to predict the fragility index of liquids and their T_{12}, which is a proxy to the laboratory glass transition temperature.

All code used in this work was built with reproducibility in mind, using open-source Python modules. Both data and code are available for anyone interested, at no cost, and with a permissive license: the hope is that this free and open framework for property prediction can be used and improved by the community to accelerate the development of new materials.

Acknowledgements

The author is thankful for the São Paulo State Research Foundation support (FAPESP grant number 2017/12491-0) as well as for the Nippon Sheet Glass overseas research grant. The author also thanks Carolina Zanelli for text revision.

Appendix

Appendix A. z-score

In the pre-processing unit of the machine learning pipeline (see Fig. 2) there is a normalization step that computes the z-score z_i of each feature that will be fed to the NN. This process (Eq. (A.1)) is performed for each feature f_i by subtracting the mean value of this feature (μ) and scaling the data to unit variance by dividing by the standard deviation of this feature (s_d).

$$z_i = \frac{f_i - \mu}{s_d} \tag{A.1}$$

Appendix B. Evaluation metrics

Four metrics were computed in Section 3.2 and are discussed here.

The coefficient of determination, R^2, has various definitions. Here it is used to test the relationship between the predicted and the reported base-10 logarithm of viscosity ($\hat{y}$ and y, respectively). The ideal relationship is a linear model with no intercept, for which the R^2 can be computed via Eq. (B.1). The value of R^2 is dimensionless and between zero and one, indicating, respectively, no correlation and perfect correlation between predicted and reported viscosity values.

$$R^2 = 1 - \frac{\sum_i^n (y_i - \hat{y}_i)^2}{\sum_i^n y_i^2} \tag{B.1}$$

The root mean square error, RMSE, is a measure of the difference between y and $\hat{y}$. It is the square root of the mean square error, as can be seen in Eq. (B.2), and it has the advantage of being in the same unit as y. The lower the RMSE, the better.

$$\mathrm{RMSE} = \sqrt{\frac{1}{n}\sum_i^n (y_i - \hat{y}_i)^2} \tag{B.2}$$

The mean absolute error MAE is the average of the absolute errors. It is also a measure of the difference between y and $\hat{y}$, but differently from RMSE, each error contributes equally and the residuals are not squared. This metric has the same unit as y and is computed using Eq. (B.3). The lower the MAE, the better.

$$\mathrm{MAE} = \frac{\sum_i^n |y_i - \hat{y}_i|}{n} \tag{B.3}$$

The median absolute error MedAE is similar to MAE, but instead of computing the average residual value, it computes the median value. This metric is robust against outliers, it has the same unit as y, and is computed using Eq. (B.4). The lower the MedAE, the better.

$$\mathrm{MedAE} = \mathrm{median}\left(|y_1 - \hat{y}_1|, |y_2 - \hat{y}_2|, \ldots, |y_n - \hat{y}_n|\right) \tag{B.4}$$

Appendix C. Early stopping routine

Neural networks can be trained for a specified number of epochs or until some stopping condition occurs. In this work, the NNs were trained for 200 epochs or until meeting the conditions of the early stopping routine. The early stopping routine looks for the validation set loss after each epoch and stops the training if no improvement has occurred in the previous P epochs. The hyperparameter P is called patience.

Appendix D. Chemical features considered in the final model

The 87 chemical features that were used in the final model are shown here using the internal notation of the code [59], for example:

- "abs|atomic_number|std" meaning that an absolute vector $\boldsymbol{A}$ was computed by considering the atomic number of the chemical elements in the liquid, and the standard deviation of vector $\boldsymbol{A}$ was then computed and stored as a feature;
- "wei|boiling_point|max" meaning that a weighted vector $\boldsymbol{W}$ was computed by considering the boiling point of the chemical elements in the liquid, and the maximum value of vector $\boldsymbol{W}$ was then computed and stored as a feature.

The features are

- abs|atomic_number|std,
- abs|atomic_radius_rahm|max,
- abs|atomic_radius_rahm|mean,
- abs|atomic_radius_rahm|std,
- abs|atomic_weight|std,
- abs|boiling_point|sum,
- abs|boiling_point|mean,
- abs|boiling_point|std,
- abs|covalent_radius_pyykko|std,
- abs|covalent_radius_pyykko_double|mean,
- abs|density|std,
- abs|dipole_polarizability|sum,
- abs|electrons|std,
- abs|en_ghosh|sum,
- abs|heat_of_formation|sum,
- abs|heat_of_formation|min,
- abs|heat_of_formation|mean,
- abs|heat_of_formation|std,
- abs|lattice_constant|mean,

- abs|lattice_constant|std,
- abs|mass_number|std,
- abs|melting_point|sum,
- abs|melting_point|mean,
- abs|melting_point|std,
- abs|mendeleev_number|min,
- abs|neutrons|std,
- abs|protons|std,
- abs|vdw_radius_alvarez|std,
- abs|vdw_radius_uff|min,
- abs|vdw_radius_uff|max,
- abs|vdw_radius_uff|mean,
- wei|atomic_number|sum,
- wei|atomic_radius|max,
- wei|atomic_radius_rahm|sum,
- wei|atomic_radius_rahm|max,
- wei|atomic_volume|sum,
- wei|atomic_volume|max,
- wei|atomic_volume|std,
- wei|atomic_weight|sum,
- wei|boiling_point|sum,
- wei|boiling_point|max,
- wei|boiling_point|mean,
- wei|boiling_point|std,
- wei|c6_gb|sum,
- wei|c6_gb|min,
- wei|c6_gb|max,
- wei|c6_gb|std,
- wei|density|sum,
- wei|density|max,
- wei|density|mean,
- wei|density|std,
- wei|dipole_polarizability|min,
- wei|dipole_polarizability|max,
- wei|dipole_polarizability|std,
- wei|electrons|sum,
- wei|en_ghosh|max,
- wei|en_pauling|max,
- wei|en_pauling|std,
- wei|glawe_number|max,
- wei|heat_of_formation|sum,
- wei|heat_of_formation|std,
- wei|lattice_constant|sum,
- wei|lattice_constant|max,
- wei|lattice_constant|std,
- wei|mass_number|sum,
- wei|melting_point|sum,
- wei|melting_point|min,
- wei|melting_point|max,
- wei|melting_point|mean,
- wei|melting_point|std,
- wei|mendeleev_number|sum,
- wei|mendeleev_number|max,
- wei|neutrons|sum,
- wei|neutrons|max,
- wei|neutrons|std,
- wei|pettifor_number|sum,
- wei|pettifor_number|max,
- wei|protons|sum,
- wei|vdw_radius|sum,
- wei|vdw_radius|max,
- wei|vdw_radius_alvarez|sum,
- wei|vdw_radius_alvarez|max,
- wei|vdw_radius_batsanov|max,
- wei|vdw_radius_mm3|max,
- wei|vdw_radius_uff|sum,
- wei|vdw_radius_uff|max,
- and wei|vdw_radius_uff|mean.

References

[1] U. Fotheringham, Viscosity of Glass and Glass-Forming Melts, in: J. D. Musgraves, J. Hu, L. Calvez (Eds.), Springer Handbook of Glass, Springer Handbooks, Springer International Publishing, Cham, 2019, pp. 79–112.

[2] M. L. F. Nascimento, E. D. Zanotto, Does viscosity describe the kinetic barrier for crystal growth from the liquidus to the glass transition?, The Journal of Chemical Physics 133 (17) (2010) 174701. doi:10.1063/1.3490793.

[3] M. L. F. Nascimento, V. M. Fokin, E. D. Zanotto, A. S. Abyzov, Dynamic processes in a silicate liquid from above melting to below the glass transition., The Journal of chemical physics 135 (19) (2011) 194703. doi:10.1063/1.3656696.

[4] D. R. Cassar, R. F. Lancelotti, R. Nuernberg, M. L. F. Nascimento, A. M. Rodrigues, L. T. Diz, E. D. Zanotto, Elemental and cooperative diffusion in a liquid, supercooled liquid and glass resolved, The Journal of Chemical Physics 147 (1) (2017) 014501. doi:10.1063/1.4986507.

[5] D. R. Cassar, A. M. Rodrigues, M. L. F. Nascimento, E. D. Zanotto, The diffusion coefficient controlling crystal growth in a silicate glass-former, International Journal of Applied Glass Science 9 (3) (2018) 373–382. doi:10.1111/ijag.12319.

[6] J. Jiusti, E. D. Zanotto, D. R. Cassar, M. R. B. Andreeta, Viscosity and liquidus-based predictor of glass-forming ability of oxide glasses, Journal of the American Ceramic Society 103 (2) (2020) 921–932. doi:10.1111/jace.16732.

[7] Z. Liu, Perspective on Materials Genome®, Chinese Science Bulletin 59 (15) (2014) 1619–1623. doi:10.1007/s11434-013-0072-x.

[8] J. C. Mauro, Decoding the glass genome, Current Opinion in Solid State and Materials Science 22 (2) (2018) 58–64. doi:10.1016/j.cossms.2017.09.001.

[9] J. C. Mauro, A. Tandia, K. D. Vargheese, Y. Z. Mauro, M. M. Smedskjaer, Accelerating the Design of Functional Glasses through Modeling, Chemistry of Materials 28 (12) (2016) 4267–4277. doi:10.1021/acs.chemmater.6b01054.

[10] E. D. Guire, L. Bartolo, R. Brindle, R. Devanathan, E. C. Dickey, J. Fessler, R. H. French, U. Fotheringham, M. Harmer, E. Lara-Curzio, S. Lichtner, E. Maillet, J. Mauro, M. Mecklenborg, B. Meredig, K. Rajan, J. Rickman, S. Sinnott, C. Spahr, C. Suh, A. Tandia, L. Ward, R. Weber, Data-driven glass/ceramic science research: Insights from the glass and ceramic and data science/informatics communities, Journal of the American Ceramic Society 102 (11) (2019) 6385–6406. doi:10.1111/jace.16677.

[11] H. Liu, Z. Fu, K. Yang, X. Xu, M. Bauchy, Machine learning for glass science and engineering: A review, Journal of Non-Crystalline Solids (2019) 119419doi:10.1016/j.jnoncrysol.2019.04.039.

[12] A. Tandia, M. C. Onbasli, J. C. Mauro, Machine Learning for Glass Modeling, in: J. D. Musgraves, J. Hu, L. Calvez (Eds.), Springer Handbook of Glass, Springer Handbooks, Springer International Publishing, Cham, 2019, pp. 1157–1192.

[13] C. Dreyfus, G. Dreyfus, A machine learning approach to the estimation of the liquidus temperature of glass-forming oxide blends, Journal of Non-Crystalline Solids 318 (1-2) (2003) 63–78. doi:10.1016/S0022-3093(02)01859-8.

[14] D. S. Brauer, C. Rüssel, J. Kraft, Solubility of glasses in the system P_2O_5–CaO–MgO–Na_2O–TiO_2: Experimental and modeling using artificial neural networks, Journal of Non-Crystalline Solids 353 (3) (2007) 263–270. doi:10.1016/j.jnoncrysol.2006.12.005.

[15] O. Bošák, S. Minárik, V. Labaš, Z. Ančíková, P. Koštial, O. Zimnỳ, M. Kubliha, M. Poulain, M. T. Soltani, Artificial neural network analysis of optical measurements of glasses based on Sb_2O_3, Journal of optoelectronics and advanced materials 18 (3-4) (2016) 240–247.

[16] N. M. Anoop Krishnan, S. Mangalathu, M. M. Smedskjaer, A. Tandia, H. Burton, M. Bauchy, Predicting the dissolution kinetics of silicate glasses using machine learning, Journal of Non-Crystalline Solids 487 (2018) 37–45. doi:10.1016/j.jnoncrysol.2018.02.023.

[17] D. R. Cassar, A. C. P. L. F. de Carvalho, E. D. Zanotto, Predicting glass transition temperatures using neural networks, Acta Materialia 159 (2018) 249–256. doi:10.1016/j.actamat.2018.08.022.

[18] J. Ruusunen, Deep Neural Networks for Evaluating the Quality of Tempered Glass, M.Sc Dissertation, Tampere University of Technology, Tampere (2018).

[19] S. Bishnoi, S. Singh, R. Ravinder, M. Bauchy, N. N. Gosvami, H. Kodamana, N. M. A. Krishnan, Predicting Young's modulus of oxide glasses with sparse datasets using machine learning, Journal of Non-Crystalline Solids 524 (2019) 119643. arXiv:1902.09776, doi:10.1016/j.jnoncrysol.2019.119643.

[20] K. Yang, X. Xu, B. Yang, B. Cook, H. Ramos, N. M. A. Krishnan, M. M. Smedskjaer, C. Hoover, M. Bauchy, Predicting the Young's Modulus of Silicate Glasses using High-Throughput Molecular Dynamics Simulations and Machine Learning, Scientific Reports 9 (1) (2019) 8739. arXiv:1901.09323, doi:10.1038/s41598-019-45344-3.

[21] E. Alcobaça, S. M. Mastelini, T. Botari, B. A. Pimentel, D. R. Cassar, A. C. P. d. L. F. de Carvalho, E. D. Zanotto, Explainable Machine Learning Algorithms For Predicting Glass Transition Temperatures, Acta Materialia 188 (2020) 92–100. doi:10.1016/j.actamat.2020.01.047.

[22] B. Deng, Machine learning on density and elastic property of oxide glasses driven by large dataset, Journal of Non-Crystalline Solids 529 (2020) 119768. doi:10.1016/j.jnoncrysol.2019.119768.

[23] T. Han, N. Stone-Weiss, J. Huang, A. Goel, A. Kumar, Machine learning as a tool to design glasses with controlled dissolution for healthcare applications, Acta Biomaterialia 107 (2020) 286–298. doi:10.1016/j.actbio.2020.02.037.

[24] J. N. P. Lillington, T. L. Goût, M. T. Harrison, I. Farnan, Predicting radioactive waste glass dissolution with machine learning, Journal of Non-Crystalline Solids 533 (2020) 119852. doi:10.1016/j.jnoncrysol.2019.119852.

[25] M. C. Onbaşlı, A. Tandia, J. C. Mauro, Mechanical and Compositional Design of High-Strength Corning Gorilla® Glass, in: W. Andreoni, S. Yip (Eds.), Handbook of Materials Modeling: Applications: Current and Emerging Materials, Springer International Publishing, Cham, 2020, pp. 1997–2019.

[26] R. Ravinder, K. H. Sridhara, S. Bishnoi, H. S. Grover, M. Bauchy, Jayadeva, H. Kodamana, N. M. A. Krishnan, Deep learning aided rational design of oxide glasses, Materials Horizons 7 (7) (2020) 1819–1827. arXiv:1912.11582, doi:10.1039/D0MH00162G.

[27] J. C. Mauro, Y. Yue, A. J. Ellison, P. K. Gupta, D. C. Allan, Viscosity of glass-forming liquids., Proceedings of the National Academy of Sciences of the United States of America 106 (47) (2009) 19780–19784. doi:10.1073/pnas.0911705106.

[28] S. Kaufman, S. Rosset, C. Perlich, O. Stitelman, Leakage in data mining: Formulation, detection, and avoidance, ACM Transactions on Knowledge Discovery from Data 6 (4) (2012) 15:1–15:21. doi:10.1145/2382577.2382579.

[29] C. C. Aggarwal, Neural Networks and Deep Learning: A Textbook, Springer International Publishing, 2018. doi:10.1007/978-3-319-94463-0.

[30] C. A. Angell, Strong and fragile liquids, in: K. L. Ngai, G. B. Wright (Eds.), Relaxation in Complex Systems, Naval Research Laboratory, Springfield, 1985, pp. 3–12.

[31] J. C. Slater, Atomic Radii in Crystals, The Journal of Chemical Physics 41 (10) (1964) 3199–3204. doi:10.1063/1.1725697.

[32] M. Rahm, R. Hoffmann, N. W. Ashcroft, Atomic and Ionic Radii of Elements 1–96, Chemistry – A European Journal 22 (41) (2016) 14625–14632. doi:10.1002/chem.201602949.

[33] M. Rahm, R. Hoffmann, N. W. Ashcroft, Corrigendum: Atomic and Ionic Radii of Elements 1–96, Chemistry – A European Journal 23 (16) (2017) 4017–4017. doi:10.1002/chem.201700610.

[34] T. Gould, T. Bučko, C_6 Coefficients and Dipole Polarizabilities

for All Atoms and Many Ions in Rows 1–6 of the Periodic Table, Journal of Chemical Theory and Computation 12 (8) (2016) 3603–3613. doi:10.1021/acs.jctc.6b00361.

[35] P. Pyykkö, M. Atsumi, Molecular Single-Bond Covalent Radii for Elements 1–118, Chemistry – A European Journal 15 (1) (2009) 186–197. doi:10.1002/chem.200800987.

[36] P. Pyykkö, M. Atsumi, Molecular Double-Bond Covalent Radii for Elements Li–E112, Chemistry – A European Journal 15 (46) (2009) 12770–12779. doi:10.1002/chem.200901472.

[37] D. C. Ghosh, A new scale of electronegativity based on absolute radii of atoms, Journal of Theoretical and Computational Chemistry 04 (01) (2005) 21–33. doi:10.1142/S0219633605001556.

[38] W. M. Haynes, CRC Handbook of Chemistry and Physics, CRC Press, 2014.

[39] D. G. Pettifor, A chemical scale for crystal-structure maps, Solid State Communications 51 (1) (1984) 31–34. doi:10.1016/0038-1098(84)90765-8.

[40] H. Glawe, A. Sanna, E. K. U. Gross, M. A. L. Marques, The optimal one dimensional periodic table: A modified Pettifor chemical scale from data mining, New Journal of Physics 18 (9) (2016) 093011. doi:10.1088/1367-2630/18/9/093011.

[41] A. K. Rappe, C. J. Casewit, K. S. Colwell, W. A. Goddard, W. M. Skiff, UFF, a full periodic table force field for molecular mechanics and molecular dynamics simulations, Journal of the American Chemical Society 114 (25) (1992) 10024–10035. doi:10.1021/ja00051a040.

[42] N. L. Allinger, X. Zhou, J. Bergsma, Molecular mechanics parameters, Journal of Molecular Structure: THEOCHEM 312 (1) (1994) 69–83. doi:10.1016/S0166-1280(09)80008-0.

[43] S. S. Batsanov, Van der Waals Radii of Elements, Inorganic Materials 37 (9) (2001) 871–885. doi:10.1023/A:1011625728803.

[44] S. Alvarez, A cartography of the van der Waals territories, Dalton Transactions 42 (24) (2013) 8617–8636. doi:10.1039/C3DT50599E.

[45] Ł. Mentel, mendeleev – A Python resource for properties of chemical elements, ions and isotopes (2020).

[46] G. Adam, J. H. Gibbs, On the temperature dependence of cooperative relaxation properties in glass-forming liquids, The Journal of Chemical Physics 43 (1) (1965) 139–146. doi:10.1063/1.1696442.

[47] J. Bergstra, D. Yamins, D. Cox, Making a science of model search: Hyperparameter optimization in hundreds of dimensions for vision architectures, in: International Conference on Machine Learning, 2013, pp. 115–123.

[48] J. S. Bergstra, R. Bardenet, Y. Bengio, B. Kégl, Algorithms for hyper-parameter optimization, in: Advances in Neural Information Processing Systems, 2011, pp. 2546–2554.

[49] J. Kiefer, J. Wolfowitz, Stochastic Estimation of the Maximum of a Regression Function, Annals of Mathematical Statistics 23 (3) (1952) 462–466. doi:10.1214/aoms/1177729392.

[50] H. E. Robbins, A Stochastic Approximation Method, The Annals of Mathematical Statistics 22 (3) (1951) 400–407. doi:10.1214/aoms/1177729586.

[51] F. Pedregosa, G. Varoquaux, A. Gramfort, V. Michel, B. Thirion, O. Grisel, M. Blondel, P. Prettenhofer, R. Weiss, V. Dubourg, J. Vanderplas, A. Passos, D. Cournapeau, M. Brucher, M. Perrot, E. Duchesnay, Scikit-learn: Machine Learning in Python, Journal of Machine Learning Research 12 (2011) 2825–2830.

[52] W. Falcon, PyTorchLightning/pytorch-lightning, Pytorch Lightning (2020).

[53] A. Paszke, S. Gross, F. Massa, A. Lerer, J. Bradbury, G. Chanan, T. Killeen, Z. Lin, N. Gimelshein, L. Antiga, A. Desmaison, A. Kopf, E. Yang, Z. DeVito, M. Raison, A. Tejani, S. Chilamkurthy, B. Steiner, L. Fang, J. Bai, S. Chintala, PyTorch: An imperative style, high-performance deep learning library, in: H. Wallach, H. Larochelle, A. Beygelzimer, F. dAlché-Buc, E. Fox, R. Garnett (Eds.), Advances in Neural Information Processing Systems 32, Curran Associates, Inc., 2019, pp. 8024–8035.

[54] W. McKinney, Data structures for statistical computing in Python, in: Proceedings of the 9th Python in Science Conference, Vol. 1, Austin, Texas, 2010, pp. 51–56.

[55] P. Richet, Y. Bottinga, Anorthite, andesine, wollastonite, diopside, cordierite and pyrope: Thermodynamics of melting, glass transitions, and properties of the amorphous phases, Earth and Planetary Science Letters 67 (3) (1984) 415–432. doi:10.1016/0012-821X(84)90179-1.

[56] S. Reinsch, M. L. F. Nascimento, R. Müller, E. D. Zanotto, Crystal growth kinetics in cordierite and diopside glasses in wide temperature ranges, Journal of Non-Crystalline Solids 354 (52-54) (2008) 5386–5394. doi:10.1016/j.jnoncrysol.2008.09.007.

[57] R. M. C. V. Reis, E. D. Zanotto, Simple model for particle phase transformation kinetics, Acta Materialia 154 (2018) 228–236. doi:10.1016/j.actamat.2018.05.039.

[58] D. R. Cassar, drcassar/glasspy: GlassPy 0.3, Zenodo (2020). doi:10.5281/zenodo.3930351.

[59] D. R. Cassar, drcassar/viscosity-graybox-nn: Viscosity Graybox NN v1.0, Zenodo (2020). doi:10.5281/zenodo.3932251.